




Oral formulation of Wnt inhibitor complex reduces inflammation and fibrosis in intraperitoneal implants in vivo

Ana Luíza de Castro Santos¹ · Natália Jordana Alves da Silva¹ · Celso Tarso Rodrigues Viana¹ · Letícia Cristine Cardoso dos Santos⁴ · Gabriel Henrique Costa da Silva¹ · Sérgio Ricardo Aluotto Scalzo Júnior¹ · Pedro Augusto Carvalho Costa¹ · Walison Nunes da Silva¹ · Itamar Couto Guedes de Jesus¹ · Alexander Birbrair⁴ · Mariana T. Q. de Magalhães² · Frédéric Frézard¹ · Silvia Guatimosim¹ · Rebecca M. Haley³ · Michael J. Mitchell³ · Silvia Passos Andrade¹ · Paula Peixoto Campos⁴ · Pedro Pires Goulart Guimaraes¹ 

Accepted: 24 January 2023
© Controlled Release Society 2023

Abstract

The use of implantable biomaterials to replace physiological and anatomical functions has been widely investigated in the clinic. However, the selection of biomaterials is crucial for long-term function, and the implantation of certain biomaterials can cause inflammatory and fibrotic processes, triggering a foreign body reaction that leads to loss of function and consequent need for removal. Specifically, the Wnt signaling pathway controls the healing process of the human body, and its dysregulation can result in inflammation and fibrosis, such as in peritoneal fibrosis. Here, we assessed the effects of daily oral administration of a Wnt pathway inhibitor complex (CD:LGK974) to reduce the inflammatory, fibrotic, and angiogenic processes caused by intraperitoneal implants. CD:LGK974 significantly reduced the infiltration of immune cells and release of inflammatory cytokines in the implant region compared to the control groups. Furthermore, CD:LGK974 inhibited collagen deposition and reduced the expression of pro-fibrotic α -SMA and TGF- β 1, confirming fibrosis reduction. Finally, the CD:LGK974 complex decreased VEGF levels and both the number and area of blood vessels formed, suggesting decreased angiogenesis. This work introduces a potential new application of the Wnt inhibitor complex to reduce peritoneal fibrosis and the rejection of implants at the intraperitoneal site, possibly allowing for longer-term functionality of existing clinical biomaterials.

Keywords Biomaterials · Polyether-polyurethane · Foreign body reaction · Fibrosis · Wnt pathway · LGK974

Introduction

The use of implantable biomaterials to replace physiological and anatomical functions has been widely investigated in the clinic [1, 2]. According to their function, the biomaterials used as implants can be developed from different materials such as synthetic and natural polymers. Of these, polyethylene (PE), polyglycolic acid (PGA), polylactic acid (PLA), poly(lactic acid-co-glycolic acid) (PLGA), and polyether-polyurethane, hyaluronic acid, chitosan, and alginate are widely studied as biomaterials for implants. Other materials, such as silicon, hydrogels, ceramics, nanofibers, and different types of metals such as silver and platinum have been also investigated and used in the clinic as implants [3, 4]. However, even with the investigation of these different biomaterial options, implant rejection is still a significant issue and limitation in the clinic, and often results in implant removal [5–7]. This rejection typically stems from

Pedro Pires Goulart Guimaraes
ppiresgo@reitoria.ufmg.br

¹ Department of Physiology and Biophysics, Institute of Biological Sciences, Federal University of Minas Gerais, Av. Pres. Antônio Carlos, 6627-Pampulha, Belo Horizonte-MG 31270-901, Brazil

² Department of Biochemistry and Immunology, Federal University of Minas Gerais, Minas Gerais, Belo Horizonte 31270-901, Brazil

³ Department of Bioengineering, University of Pennsylvania, Philadelphia, PA, USA

⁴ Department of Pathology, Institute of Biological Sciences, Federal University of Minas Gerais, Belo Horizonte-MG 31270-901, Brazil

the development of inflammatory and fibrotic processes that trigger a reaction known as the foreign body reaction [8].

To mimic the inflammatory, fibrogenic, and angiogenic responses present during typical repair processes, as well as in the foreign body reaction that biomaterial implantation can trigger, the polyether-polyurethane synthetic matrix model can be used [9–11]. This synthetic matrix consists of an acellular and avascularized polymeric structure, which allows for the infiltration of inflammatory cells, the formation of fibrotic tissue, and neovascularization [9]. Since polyurethane is a biomaterial widely used in the clinic—found in catheters, silicone prostheses, and controlled drug release systems, among others [12–15]—this implant model can be used at different sites, such as the intraperitoneal region, to assess the processes triggered after the implantation of a biomaterial in the body [9, 16]. One such potential process to evaluate is peritoneal fibrosis—a common pathological event found in more than 50% of patients with peritoneal implants such as dialysis catheters or membranes [17, 23].

Under typical conditions of tissue damage, the immune system acts to promote repair of the site that has been injured [18]. Similarly, the implantation of biomaterials, biodevices, or prostheses can initiate a foreign body reaction, leading to inflammatory and fibrotic processes [19]. This begins at the moment of implant, with the local injury triggering a continuous inflammatory process (acute phase). The next stage of the fibrosis process (chronic phase) promotes the encapsulation and isolation of the implant from the rest of the body, to encourage repair of the injured tissue [19, 20]. This process can damage the integrity of the implant and result in consequent need for removal [19, 20]. The Wnt signaling pathway plays a crucial role in tissue repair [21]. However, dysregulation in Wnt signaling can lead to fibrosis under other non-desirable conditions [21].

The Wnt pathway is divided into two branches: (1) the canonical (β -catenin-dependent) component, which primarily regulates cell proliferation and therefore tissue repair and (2) the non-canonical (β -catenin-independent and calcium-dependent), which promotes the regulation of cell polarity and movement [21, 22]. It has been reported that dysregulation of the Wnt/ β -catenin pathway contributes to fibrosis processes in several tissues [21–24]. Furthermore, it was demonstrated that specific Wnt ligands are responsible to induce fibrosis in different tissues and cells [21]. Wnt1 and Wnt5a are the Wnt family members upregulated in peritoneal fibrosis [23]. The upregulated WNT ligands bind to a receptor complex, which is composed of FZD and LRP 5/6 receptors, resulting in β -catenin accumulation in the cytoplasm. The β -catenin will induce the transcription of excessive pro-fibrotic genes into the nucleus, such as transforming growth factor-beta 1 (TGF- β). This process generates an aberrant increase in

myofibroblast activity as well as abnormal extracellular matrix deposition in the tissue, which contributes to fibrosis [22]. Recent studies show that Wnt signaling inhibition can prevent the development of the pathological process, such as tumor progression and fibrosis, via reduction of inflammation, collagen deposition, and neovascularization [22]. One Wnt regulator, LGK974, is a small molecule developed by Novartis, currently in phase II clinical trials (NCT01351103) acting as an inhibitor of the porcupine protein and promoting Wnt ligand maturation [22].

LGK974 is currently administered orally, but has very poor solubility, limiting its bioavailability and clinical use. Recently, our group demonstrated that LGK974 complexation with cyclodextrins (CD) can improve solubility, stability, and bioavailability of the drug, as well as minimize toxicity in the gastrointestinal tract [25]. CD are naturally cyclic oligosaccharides that increase in size according to the number of glycoside monomers: 6 (α -cyclodextrins), 7 (β -cyclodextrins), and 8 (γ -cyclodextrins) [26, 27]. They have a conical shape, a hydrophobic cavity, and a hydrophilic exterior. Because of these characteristics, CD can interact with a wide range of substances, forming host–guest inclusion complexes through weak van der Waals-type interactions between the drug and the hydrophobic cavity [26–28].

Herein, we investigated the use of the complex CD:LGK974 to reduce inflammatory, fibrotic, and angiogenic processes in intraperitoneal implants of polyether-polyurethane in vivo. The Wnt pathway inhibition complex is formed by sulfobutyl-ether- β -cyclodextrin-modified cyclodextrin (β SBECD) and the insoluble drug LGK974 (CD:LGK974). Thus, we hypothesized that the orally administered CD:LGK974 complex can reduce the foreign body reaction and prevent fibrosis formation in intraperitoneal implants through inhibition of the Wnt pathway.

Material and methods

Preparation of CD:LGK974 inclusion complex

Inclusion complexes between LGK974 and β SBECD were obtained by a previously described freeze-drying technique using a CD:drug molar ratio of 10:1. LGK974 and β SBECD were dispersed in Milli-Q water, and the suspension was stirred at room temperature on a magnetic stirrer (IKA- CMAGHS7), followed by pH adjustment to \sim 4–5 using a 0.1N HCl solution, or until complete solubilization of the mixture. This mixture was kept under stirring at room temperature for 2–4 h. Next, the solution was lyophilized, and the resulting powder was stored in a freezer at $-20\text{ }^{\circ}\text{C}$ [25].

Two-dimensional nuclear magnetic resonance spectroscopy (2D-NMR)

All nuclear magnetic resonance spectroscopy (NMR) spectra were recorded at 28 °C on a Bruker® AVANCE III 600 spectrometer, operating at 600.130 MHz for ¹H measurements. The complex was dissolved in a solution containing 10% (v:v) D₂O (99.9%) at a final concentration of 3 mg/mL. The CD:LGK974 complexation was observed via nuclear Overhauser spectroscopy (NOESY) experiments using a mixing time of 650 ms. The measurements were acquired with a spectral width 9615.385 Hz in both dimensions, 1024 complex points in t₂, 256 complex points in t₁, 48 scans per increment and relaxation delay 2 s. The spectrum was processed using TopSpin 4.1.3 (academic free version). CD:LGK974 complexation and structure was determined through the correlation of proton cross-peaks observed between βSBECD (-CH-, 3–4.2 ppm) and LGK974 (aromatic -CH-, 7.7–9.2 ppm) [25].

Animal model

Male C57BL/6 mice aged 8 to 12 weeks (25–30 g), obtained from the Central Animal Facility of UFMG, were used for this work (total *N* = 68). The animals were kept throughout the treatment period in the vivarium of the Department of Physiology, Institute of Biological Sciences (ICB/UFMG), in-unit cages, ventilated racks with microisolators, under a 12-h light/dark cycle, with feed (NUVILAB CR-1 Brazil) and water *ad libitum* for 14 days. The protocols for animal experimentation were approved by the Ethics Committee at the Federal University of Minas Gerais (CEUA/UFMG) (Protocol No. 282/2018). All procedures were performed following the standards established in the guidelines and policies of the National Institutes of Health (NIH) Guide for the Care and Use of Laboratory Animals.

Preparation of sponge discs, implantation, and treatment

The peritoneal implants used were a synthetic matrix of polyether-polyurethane (Vitafoam Ltd., Manchester, UK) in a disk-shape: 5 mm thick and 8 mm in diameter (Fig. 1A–B). Implants were soaked in 70% (v/v) alcohol and sterilized in boiling distilled water for 30 min before implantation [9, 29]. Mice were anesthetized through intraperitoneal injection of ketamine (60 mg/kg) and xylazine (10 mg/kg). After ventral hair removal, aseptic technique was performed using 70% (v/v) ethanol before surgery. During the surgery procedure, a 1-cm incision was made in the midline alba of the abdomen to implant the synthetic matrix at the intraperitoneal site (Fig. 1B). After surgery, mice were sutured with non-absorbable nylon thread and

placed in individual boxes. Mice were then divided into three groups (Control, CD, and CD:LGK974) in a randomized manner. Treatment by oral administration began 24 h after implantation of synthetic matrix and continued daily for 14 days (60 μL/day): CD:LGK974 complex (dose: 5 mg/kg/day); CD equivalent dose to the complex (dose: 230 mg/kg/day); and Control (saline 0.9%) (Fig. 1C).

Sample and fluid collection

After 14 days of treatment, mice were euthanized and intraperitoneal implants were harvested, weighed, and photographed (Nikon SMZ 445 LED base stereomicroscope) at 0.67× and 5× magnification. Liver tissues were harvested for biochemical and histological analyses. Blood samples were collected for biochemical analysis.

Histopathological analyses

Harvested implants were fixed in 10% formalin for 48 h and then processed for paraffin embedding. Sections of 5-μm thickness were prepared and stained with hematoxylin and eosin (H&E) for morphometric analysis (inflammatory cells, giant cells, fibroblasts, and vessels) (Fig. S2). To assess the level of inflammation, sections were evaluated according to the following score: 0—Absent; 1—Small amount of cells present; 2—Normal amount of cells present; 3—Predominantly neutrophils present; and 4—Predominantly mononuclear cells present. To assess the level of fibrosis, collagen deposition in the sections was evaluated following the following score: 0: Absent; 1: Presence of few fine fibers; 2: Accentuated presence of fine fibers; 3: Presence of fine fibers and thick fibers; and 4: Predominance of thick collagen fibers [30, 31]. Furthermore, the number of giant cells and the number of vessels per field (15 fields per slide) were assessed using conventional microscopy (Olympus BX51) at magnification of 40x.

Immunofluorescence

Implants were harvested to prepare cryosections of 5-μm thickness. Samples were stained with CD31 (1:100, ThermoFisher) and CD68 (1:1000, ABCAM) overnight at 4 °C. Nuclei were stained with DAPI (ThermoFisher) and mounted in Dako fluorescence mounting medium (Dako, Santa Clara, CA) before images were taken using Zeiss—ApoTome.2 microscope (Oberkochen, Germany), with 40× objective and a filter-based PE (594 nm) channel at the Center for Acquisition and Processing of Images (CAPI-UFMG). Quantitative analysis was performed using ImageJ software.

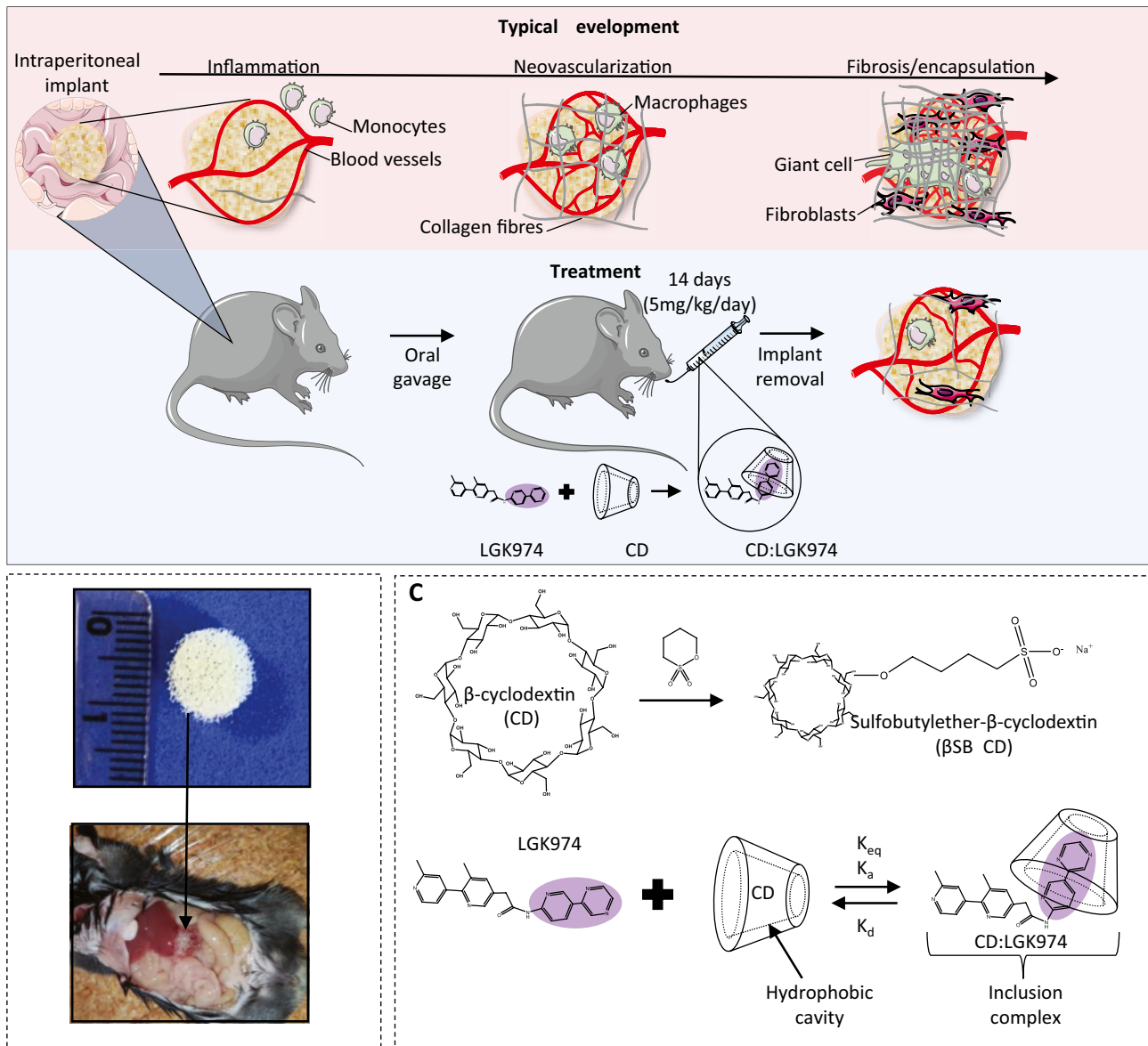


Fig. 1 Schematic of inclusion complex, synthetic matrix implantation, and CD:LGK974 treatment. **Top:** stages of foreign body reaction developed by the implantation of the polyether-polyurethane matrix. **Bottom:** schematic overview of the daily treatment with CD:LGK974 by oral gavage for 14 days. **B** Top: macroscopic image of the synthetic

polyether-polyurethane matrix before implantation. **Bottom:** implanted and adhered matrix at the intraperitoneal cavity of C57BL/6 mice. **C** Chemical structure of modified β -cyclodextrin (sulfobutylether- β -cyclodextrin) and schematic of host-guest complex under thermodynamic equilibrium

Collagen deposition evaluation

Collagen production was assessed using picosirius red stain [32]. This method allows differentiation between thick/mature collagen (red and orange to yellow birefringence) and thin/immature collagen (greenish birefringence) under polarized light, according to the degree of matrix deposition and maturity [32]. Briefly, samples were fixed in a 10% neutral buffered formalin solution for 48 h and then processed for paraffin inclusion. After cross section to 10 μm thickness, a deparaffinization step was performed in xylene and

ethanol, followed by hydration in a series of graded alcohols until distilled water, followed by incubation with a Sirius red (Sigma) solution diluted in 0.1% saturated picric acid. After 45 min at room temperature, samples were rinsed with distilled water. Sections were examined by polarization microscopy (Olympus, CX41). To quantify each collagen area type, a threshold algorithm was used to determine the red ($\text{red} > \text{green} + \text{blue} \times 1.2$) and green ($\text{green} > \text{red} + \text{blue} \times 0.7$) pixels (the multiplication factor in the formulae was determined empirically for the current image set). Then, the red and green pixels were counted to determine the tight and

thin collagen areas, respectively. To obtain the tissue area, the brightfield image was transformed into a grayscale image and binarized [33]. To segment the tissue of interest and avoid artifacts and segmentations outside of the region of interest, a combination of the Canny edge detector and morphological operations (dilation and erosion) was used [34]. The total tissue area was quantified by counting the number of white pixels in the region of interest of the binarized image. Once each collagen type and tissue pixel area were obtained, the collagen content was calculated as a percentage of the area tissue.

Determination of cytokines (TNF- α , VEGF, TGF- β 1) at the implants

To evaluate the level of cytokines tumor necrosis factor alpha (TNF- α), vascular endothelial growth factor (VEGF), and TGF- β 1 at the implants, an ELISA immunoassay was performed. Briefly, implants were homogenized in PBS (pH 7.4), and centrifuged at $10,000 \times g$ for 30 min at 4 °C. Cytokines were measured in 100 μ L of the supernatant using immunoassay kits (R & D Systems, USA), according to the manufacturer's protocol. The supernatant was then added to the ELISA plate, which was previously sensitized with a murine monoclonal antibody specific for the cytokine of interest, followed by a second polyclonal antibody conjugated to horseradish peroxidase (HRP). Following, the plate was washed to remove unbound antibody-enzyme reagents, and a colorimetric substrate solution (50 μ L of a 1:1 solution of hydrogen peroxide and tetramethylbenzidine (10 mg/mL) in dimethylsulfoxide (DMSO)) was added to the wells. After 20 min of incubation, the colorimetric reaction was stopped by adding 2N H₂SO₄ (50 μ L), and the color intensity was measured at 540 nm in a spectrophotometer (Thermoplate Tekmar). The standards used for the calibration curve (recombinant murine cytokines at 0.5-^{log}₁₀ dilutions) varied from 7.5 to 1000 pg/mL (100 μ L). The results were expressed as pg cytokine/mg wet tissue.

Western blotting

The evaluation of protein expression at the implants was performed by western blotting. Briefly, implants were homogenized on ice for 20 min in lysis buffer (NaCl, 100 mM; Tris-base, 50 mM; EDTA-2Na, 5 mM; Na₄P₂O₇ \times 10 H₂O, 50 mM; MgCl₂, 1 mM; pH 8.0) with detergents (Nonidet P40 1%, Triton x-100 0.3% and sodium deoxycholate 0.5%), containing protease inhibitors (Phenylmethylsulfonyl fluoride (PMSF) 200 mM; benzamidine 15.7 mg/mL; pepstatin 10 mM; aprotinin 10 mg/mL) and phosphatase inhibitors (NaF 20 mM; Na₃VO₄ 1 mM). Following tissue homogenization, samples were centrifuged for 12 min at 8000 rpm at 4 °C, and the supernatant was collected and stored at -80 °C

for later use. Proteins were quantified according to the Bradford method. Then, proteins (40 μ g) were separated in a 10% SDS-PAGE gel, followed by western blotting. The runs were performed with fixed voltage at 120 V and variant amperage for 1 h and 40 min. Transfer to polyvinylidene difluoride (PVDF) membrane was performed using the semi-dry apparatus (BioRad), with fixed voltage at 20 V and variant amperage for 45 min. Immediately after, the membranes were washed in tris buffered saline with Tween (TBS-T) solution (in mmol/L: NaCl, 150; Tris, 25; and 0.05% Tween 20, pH 8.0). Blocking was performed in TBS-T solution with 5% milk for 1 h at room temperature. The membranes were incubated overnight at 4 °C with primary antibody diluted in 1% milk solution in TBS-T. The following antibodies were used: β -catenin (1:1000, Invitrogen), Smooth muscle alpha-actin (α -SMA) (1:1000, ABCAM), and TGF- β 1 (1:1000, ABCAM). After incubation with the primary antibody, the membranes were washed with TBS-T for 30 min under agitation (3 times, 10 min) and incubated with the HRP secondary antibody for 1 h. The following secondary antibodies were used: anti-mouse (1:15,000, Sigma-Aldrich) and anti-goat (1:15,000, Sigma-Aldrich). After this period, the membranes were washed again with TBS-T for 30 min (3 times of 10 min). Immunodetection was performed using enhanced chemiluminescence detected with LAS 4000 equipment (GE Healthcare Life Science). Protein levels were expressed as a ratio of optical densities by analysis in ImageQuant TL[®]. HSP90 (1:3000, Santa Cruz Biotechnology) was used to normalize protein expression.

Immunophenotypic and functional features of infiltrating leukocytes

The migration of myeloid lineage cells was evaluated by immunophenotyping using flow cytometry. Harvested implants were macerated in 0.2% collagenase and then incubated at 37 °C for 30 min. Cells were centrifuged, and the resulting pellet was incubated in 0.25% trypsin for 5 min at 37 °C, after which the reaction was stopped with 10% PBS-SBF. Samples were filtered using cell strainer (40 μ m), centrifuged, and red blood cells (RBC) were lysed. Samples were resuspended in FACS buffer (PBS 1X, 0.1% BSA 2 mM azide). To assess cell viability and block nonspecific binding, cells were incubated with Live/Dead stain (Invitrogen) containing FcBlock (Invitrogen) for 15 min at room temperature and centrifuged at 2500 rpm for 3 min at 4 °C. Next, to perform extracellular labeling, cells were incubated with an antibody mix, described in supplementary materials (Table S1), for 20 min at room temperature. Samples were then centrifuged at 2500 rpm for 3 min at 4 °C and incubated with streptavidin for 15 min at room temperature. Subsequently, samples were centrifuged at 2500 rpm for 3 min at 4 °C, and the supernatant was discarded. Next, the cells

were resuspended in 200 μ L of FACS buffer and transferred to cytometry tubes. Sample acquisition was performed on a LSR Fortessa cytometer (BD), and results were analyzed using FlowJo 10 software (TreeStar).

Determination of liver toxicity

To assess liver toxicity, liver transaminases serum aspartate aminotransferase (AST) and alanine aminotransferase (ALT) were quantified on serum and liver samples. Liver samples were homogenized in 2 mL of PBS (pH 7.4). The enzymes AST and ALT were measured in the liver and serum samples using a Bioclin Kit (Copyright © 2012 Bioclin/Quibasa), following the manufacturer's protocol information, adapted for 96-well plate.

Statistical analysis

The study results are presented as mean \pm S.E.M. Analysis of statistical normality of the data was performed using GraphPad Prism 8.0 software, using One-Way ANOVA and Tukey's multiple comparison post-test. For non-parametric data, the Kruskal–Wallis test and Dunn's multiple comparison post-test were used. Values of $P < 0.05$ were considered significant.

Results

Synthesis and characterization of the CD:LGK974 inclusion complex

To characterize the host–guest interaction and CD:LGK974 complex formation (Fig. 1A), 2D NOESY-NMR was performed. The 2D correlation provides an effective interpretation of the interaction and site to characterize the complexation, considering that interactions are weak and accompanied by small chemical shift variation [35]. The set of resonances was observed indicating that the complexation occurs under fast exchange conditions relative to the NMR time scale. The 2D NOESY NMR confirmed the formation of the CD:LGK974 complex by intense cross-peaks found between the signals at 3.7 ppm of CD and 8.2–8.7 ppm of LGK974 (Fig. S1). These cross-peaks suggest that one type of complex is formed and that LGK974 might be forming inclusion complexes with CD.

Inhibition of Wnt signaling by CD:LGK974 complex reduced the inflammatory response

Twenty-four hours after implantation of the synthetic matrix at the intraperitoneal site, mice were treated with saline 0.9% (Control), β SBECD (CD), or CD:LGK974 for 14 days

(Fig. 1A). On day 14 of treatment, mice were euthanized and intraperitoneal implants were harvested.

First, we performed macroscopic analysis of the implants from mice treated with CD:LGK974. As shown in Fig. 2A–B, implants from CD:LGK974-treated mice showed less fibrotic tissue and fewer microvessels, compared to the Control and CD-treated groups. To assess the inflammation score, the infiltration of immune cells, such as neutrophils, monocytes, and macrophages was analyzed in sections of the implants stained with H&E. The level of pro-inflammatory cytokine TNF- α was also analyzed. Mice treated with CD:LGK974 presented reduced inflammatory infiltrate, resulting in a decrease of inflammation score compared to the Control and CD groups (Fig. 2C–F; Fig. S2). Furthermore, mice treated with CD:LGK974 showed a reduction in the release of pro-inflammatory cytokine TNF- α compared to the Control and CD groups (Fig. 2G).

Flow cytometry was used to assess the infiltration of myeloid lineage cells into the implant. Cells of the myeloid lineage—such as neutrophils, monocytes, macrophages pro-inflammatory or pro-fibrotic (expressing the mannose receptor CD206), and dendritic cells—are directly involved in the inflammatory response in the chronic/persistent phase of foreign-body reaction [36, 37]. Therefore, the presence or absence of myeloid cells can be used to evaluate the level of foreign-body reaction occurring. To determine the boolean gate for flow cytometry analysis, doublets were eliminated using a combination of forward scatter area (FSC-A) vs forward scatter height (FSC-H), debris of fluorochromes were discarded, and cells were gated as a function of time versus FSC-A to prevent potential interference from flow interruptions. CD45 + live cells were used for myeloid panel analysis, and within that, a gate was performed for the analysis of CD11b + (myeloid cells), dendritic cells (CD11c +), and activated dendritic cells (CD11 + IA-IE +). CD206 proportion was defined on macrophages (CD11b + F4/80 + Gr-1 +), neutrophils (CD11b + F4/80-Gr-1 +), and monocytes (CD11b + F4/80highGr-1 -). The mice group treated with CD:LGK974 exhibited significantly decreased infiltration of these immune cells to the implant compared to Control and CD groups, which highlights its anti-inflammatory potential (Fig. 3A–B). Furthermore, the pro-fibrotic phenotype (CD206 +), an important component of the chronic/persistent phase of the inflammation and fibrosis process, was evaluated in these cells. The CD:LGK974 treated-group exhibited reduced infiltration of cells expressing CD206 (mannose receptor). Together, these results demonstrate that CD:LGK974 decreased expression of pro-inflammatory cytokines and consequently reduced the infiltration of both pro-inflammatory and pro-fibrotic myeloid immune cells to the implant.

Giant cells are composed of macrophage clusters which combine to form multinucleated cells with greater

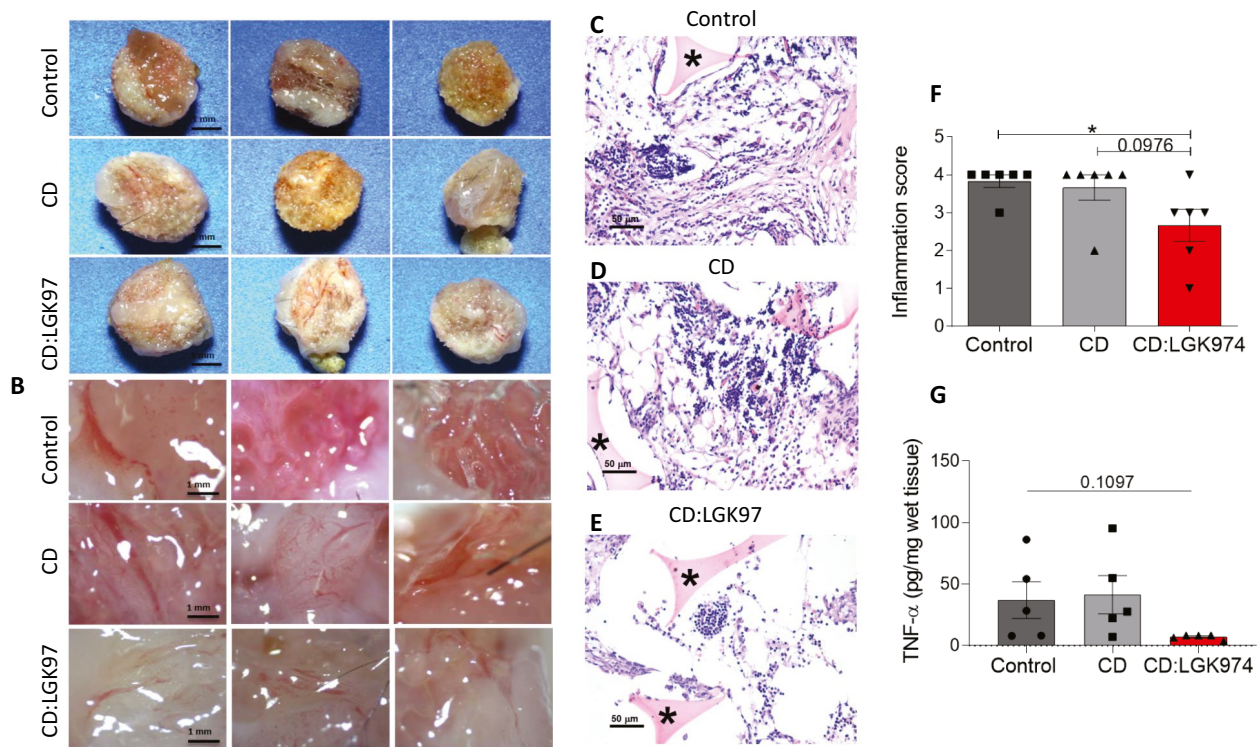


Fig. 2 CD:LGK974 complex treatment reduced inflammation in the polyether-polyurethane implant. Representative images of implants treated with Control: saline, CD, and CD:LGK974 (from top to bottom) for 14 days, 6.7×magnification. **B** Representative images of implants were focused at 5×magnification. Scale bar, 1 mm. **C–E** Representative histological sections of implants stained with H&E after 14 days of oral treatment (portions of implant matrix indicated

by *). **C** Control: saline; **D** CD; **E** CD:LGK974 (dose: 5 mg/kg/day). Scale bar, 50 μ m. **F** CD:LGK974-treated group decreased implant-induced inflammatory infiltration compared to Control and CD groups. **G** CD:LGK974-treated group decreased release of pro-inflammatory cytokine TNF- α compared to Control and CD groups. Data are expressed as mean \pm S.E.M.; One-way ANOVA * $P < 0.05$

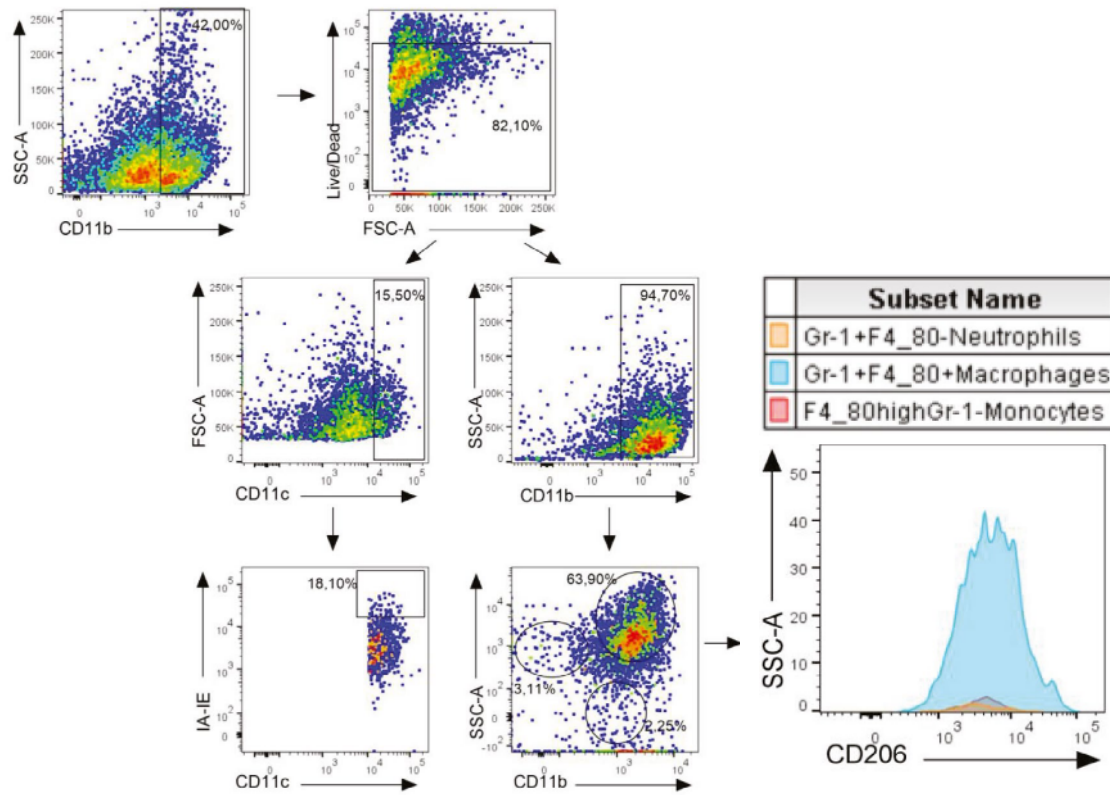
phagocytosis capacity. These giant cells accumulate during the end-stage response of the foreign-body reaction, working to surround and isolate the foreign body, such as implants at the intraperitoneal site [36]. Mice treated with CD:LGK974 complex showed a significantly decreased number of CD68 positive giant cells formed at the implant compared to Control and CD groups (Fig. 4A–H).

Inhibition of Wnt signaling with CD:LGK974 complex decreased implant fibrosis

To investigate the occurrence of fibrosis at the implant, we analyzed the fibrosis score in histological sections of the implant, as well as the production of pro-fibrotic cytokines, expression of fibrosis-related proteins, and collagen deposition. The fibrotic score was determined by the level of fibrotic tissue deposition at the implant matrix. Mice treated with CD:LGK974 demonstrated a significant reduction—compared to Control and CD—in the deposition of implant-associated fibrotic tissue (Fig. 5A–D), the release of the pro-fibrotic cytokine TGF- β 1 (Fig. 5E), and the expression

of β -catenin protein, a nuclear transcription cofactor of the Wnt pathway (Fig. 5G). CD:LGK974 treated-group also decreased α -SMA and TGF- β 1 expression compared to Control and CD (Fig. 5H–I). These results all suggest that inhibition of the Wnt pathway was effective in reducing pro-fibrotic factors as well as extracellular matrix deposition at the implants (Fig. 5F–I; Fig. S3).

Fibrosis is characterized by persistent inflammation to repair tissue in a delayed manner or through cicatrization—scar formation—by which normal tissue is replaced with connective tissue through the exacerbated deposition of extracellular matrix such as collagen [19, 36]. The collagen deposited during the fibrosis process consists of collagen type III (thinnest)—the first collagen to be deposited—and collagen type I (thickest). To assess the deposition of type I (red/orange) and type III (green) collagen, we analyzed stained sections with picrosirius by using polarized light (Fig. S4). Mice treated with CD:LGK974 complex significantly decreased total collagen and type I collagen deposition compared to the Control and CD groups, which indicated a considerable reduction of fibrosis formation at



B

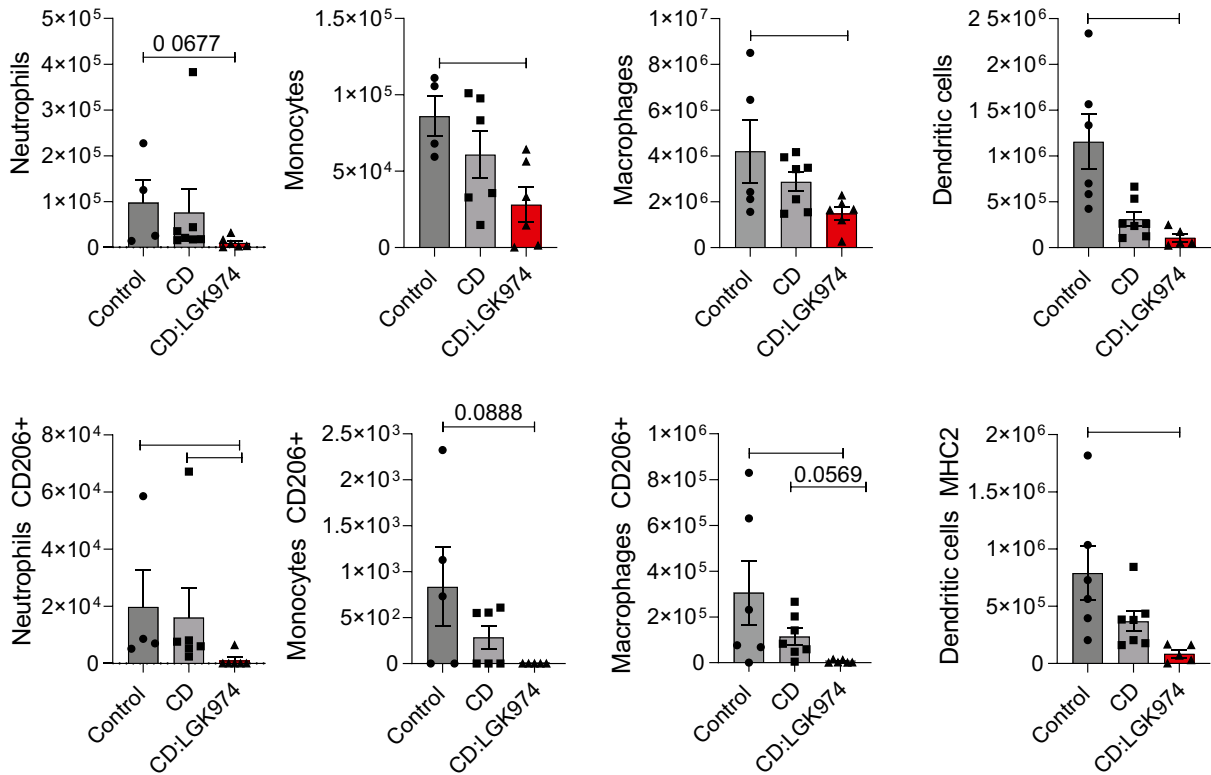


Fig. 3 Inhibition of Wnt signaling by CD:LGK974 complex modulates myeloid cell infiltration. **A** Representative large dot image of the gating strategy used to obtain myeloid cell records. **B** Number of myeloid cells at the implant. Neutrophils (CD11b+,F4/80-,Gr-1+), CD206+neutrophils (F4/80-,Gr-1+,CD206+), monocytes (CD11b+,F4/80high,Gr-1-), and CD206+ monocytes (F4/80high,Gr-1-,CD206+), macrophages (CD11b+,F4/80+,Gr-1+), CD206+ macrophages (F4/80+,Gr-1+,CD206+), dendritic cells (CD11c+), activated dendritic cells (CD11c+,IA-IE+). In all conditions, CD:LGK974 significantly decreased cell infiltration to the implant compared to Control group and CD groups. Data are mean \pm S.E.M.; One-way ANOVA; * $P < 0.05$; ** $P < 0.01$

the implant. Furthermore, there was no difference in type III collagen deposition between the groups (Fig. 6A–B). Collectively, these results indicate that mice treated with CD:LGK974 have reduced deposition of both type I and total collagen at the implant.

CD:LGK974 treatment alters the angiogenic profile of implants

The formation of fibrovascular tissue is a result of the inflammatory process triggered by the implant and leads to the release of pro-angiogenic factors such as VEGF and PDGF (platelet-derived growth factor). These factors have a crucial role in the formation of new vessels, which will feed the surrounding tissue and allow for the infiltration of inflammatory cells which encapsulate and isolate the biomaterial [9, 10, 19, 38]. To investigate the angiogenesis process that occurs after implant, we assessed the number of vessels, their area, and the production of pro-angiogenic factor VEGF. The evaluation of new vessels formation was performed through morphometric analysis of the H&E-stained sections and immunofluorescence analysis, counting the number of vessels per field and their area (15 fields per slide–40 \times). Treatment with CD:LGK974 reduced both the number and area of vessels compared to Control and CD groups (Fig. 7A–H). Moreover, mice treated with CD:LGK974 exhibited decreased production of the pro-angiogenic cytokine VEGF compared to other groups, supporting the general findings of a reduced foreign body reaction after treatment with CD:LGK974 (Fig. 7I).

Liver transaminases measurement

Liver transaminases are essential biomarkers of liver damage that, when elevated, may indicate a damaging process in the liver [39]. To assess whether treatment with the CD:LGK974 complex induces liver toxicity, levels of alanine aminotransferases (ALT) and aspartate aminotransferases (AST) enzymes were measured. The levels of AST and ALT were evaluated in serum and liver fragments of animals from each experimental group. There was no difference in the levels of

AST or ALT between mice treated with CD:LGK974 compared to Control and CD groups, indicating no liver toxicity due to CD:LGK974 treatment (Fig. S5).

Discussion

The application of biomaterials in clinical practice is extremely broad, including cell transplantation, controlled drug release, replacement of anatomical structures, monitoring of physiological conditions, and tissue regeneration [7, 40]. However, the performance of these biomaterials, including implants, depends on their interaction with immune system components [7], beginning at the moment of implantation, which causes injury to the local tissue. At first, this injury causes inflammation—to repair the injured tissue—but over time, this reaction can become persistent, triggering a process known as foreign body reaction. This can damage the implant through the encapsulation of the biomaterial by fibrotic tissue, causing loss of function, pain, and discomfort to the patient [7, 8].

The implantation site greatly influences the inflammatory reactions triggered by the implanted biomaterial. The intraperitoneal site has great inflammatory potential due to the extensive vascularization and the presence of peritoneal fluid, enabling the rapid recruitment of large quantities of inflammatory cells such as macrophages and lymphocytes to the site of inflammation [16]. Moreover, implants can be extensively adhered to the adjacent visceral organs, which may promote the infiltration of not only inflammatory cells but also of fibroblasts [16]. The implantation of the polyether-polyurethane matrix at intraperitoneal site can be used to mimic the inflammatory response and stages of tissue repair that typically affect an implant [9, 29]. Here, the polyether-polyurethane matrix was implanted at the intraperitoneal site of mice to mimic the development of the foreign body reaction. Inflammation at the intraperitoneal space is highly relevant in cases such as peritoneal fibrosis, a deleterious pathologic event that is quite common in patients with peritoneal dialysis. When peritoneal fibrosis occurs, it causes failure and discontinuation of this otherwise lifesaving treatment. Infectious peritonitis is another condition which induces angiogenesis and fibrosis and is a major cause of morbidity and mortality in patients with peritoneal dialysis [17]. If these inflammatory events could be slowed or stopped entirely, the lifetime of these biomaterials could be extended, in turn, extending the usage of these vital treatments.

The process of fibrosis has been correlated with dysregulation of the Wnt pathway in several tissues [21]. The Wnt pathway plays a key role in proliferation, cell differentiation, and tissue repair [41, 42]. To limit the development of foreign body reaction in intraperitoneal implants,

we assessed the effects of Wnt pathway inhibition. In this work, Wnt inhibition was achieved via daily oral treatment with CD:LGK974 complex. LGK974 is a blocker of the canonical component of the Wnt pathway, which reduces the accumulation of β -catenin in the cytoplasm and causes decreased nuclear translocation and expression of pro-fibrotic genes. However, due to its strong hydrophobicity, LGK974 has low solubility in aqueous solvents, which limits its clinical use. Toxic body effects after oral administration have also been reported [25, 41]. To overcome these limitations, we used a previously reported CD:LGK974 complex, which is a supramolecular compound using CD

Fig. 5 Fibrosis in implants is decreased by oral treatment of CD:LGK974 complex. **–C** Representative histological sections of implants after 14 days of oral treatment, stained by H&E (portions of the implant matrix are indicated by *). **Control:** saline; **B** CD; **C** CD:LGK974 (dose: 5 mg/kg/day). Scale bar, 50 μ m. **D** Treatment with CD:LGK974 significantly decreased fibrosis at the implants compared to Control and CD groups. **E** CD:LGK974 significantly reduced pro-fibrotic cytokine TGF- β 1 compared to Control and CD groups. **F** Representative images of semiquantitative analysis by western blotting of β -catenin, α -SMA, and TGF- β 1 in intraperitoneal implants normalized by HSP90. **G–I** Treatment with CD:LGK974 complex decreased β -catenin and pro-fibrotic α -SMA and TGF- β 1 in intraperitoneal implants. Data are mean \pm S.E.M.; One-way ANOVA with Dunnett correction for multiple comparisons; * P < 0.05

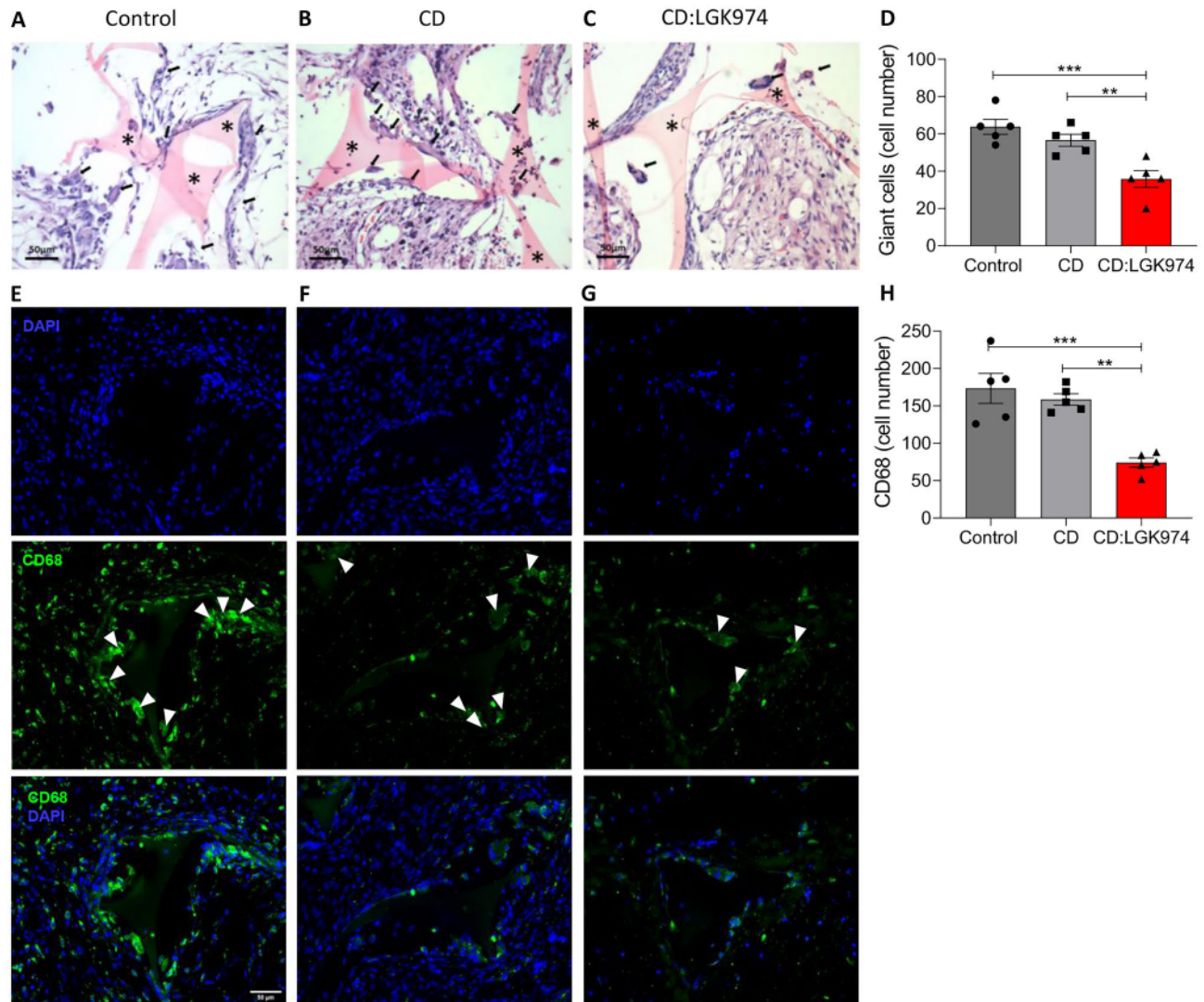


Fig. 4 Giant cell formation is reduced after CD:LGK974 treatment. **–C** Representative histological sections of implants 14 days after oral treatment (portions of implant matrix are indicated by *). **Control:** saline; **B** CD; **C** CD:LGK974 (dose: 5 mg/kg/day). **D** Morphometric analysis of giant cells/field (indicated by arrows) showed that CD:LGK974 had a significantly decreased number of giant cells formed at the implant compared to Control and CD groups. **E–G** Representative

immunofluorescence of CD68 at the implants 14 days after oral treatment. **E** Control: saline; **F** CD; **G** CD:LGK974 (dose: 5 mg/kg/day). Scale bar, 50 μ m. **H** Fluorescence quantification of CD68+cells/field (indicated by arrows) showed that CD:LGK974 had a significantly decreased CD68+cell number at the implant compared to Control and CD groups. Data are mean \pm S.E.M.; One-way ANOVA; ** P < 0.01; *** P < 0.001

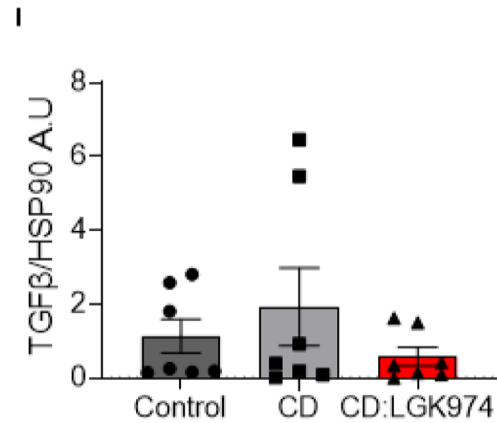
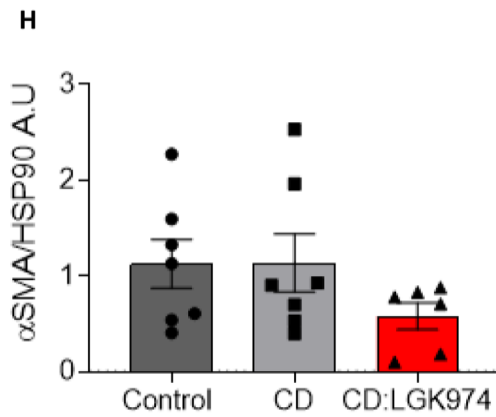
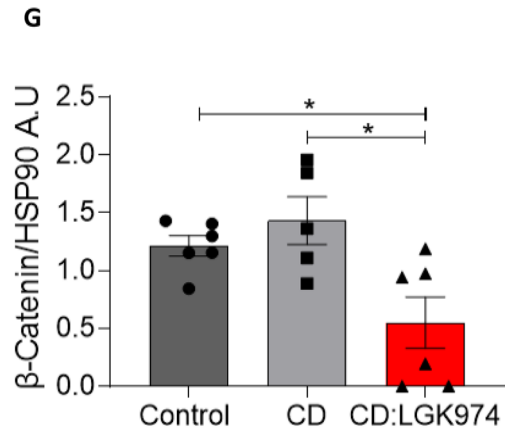
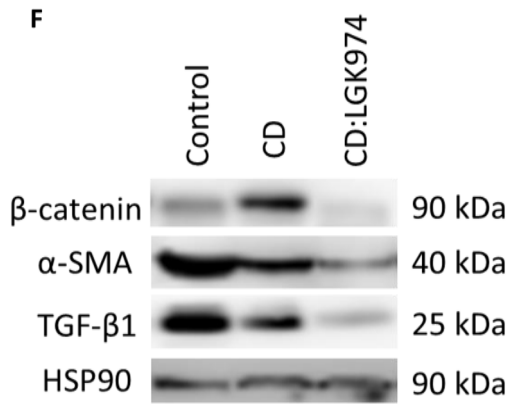
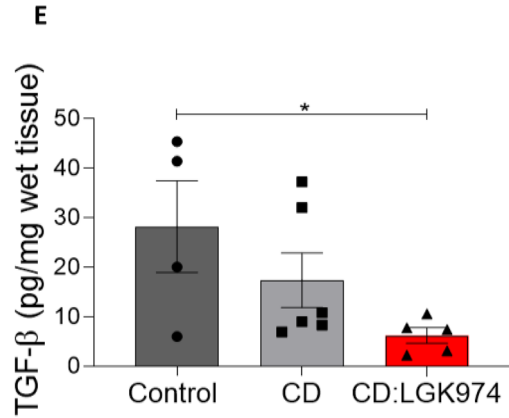
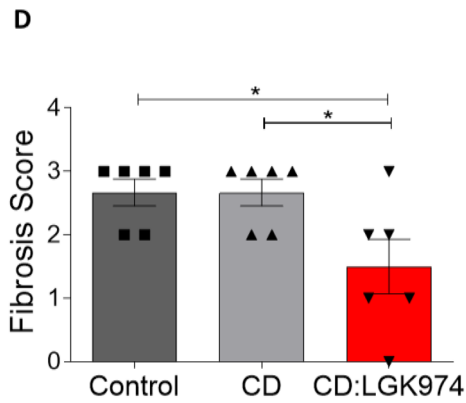
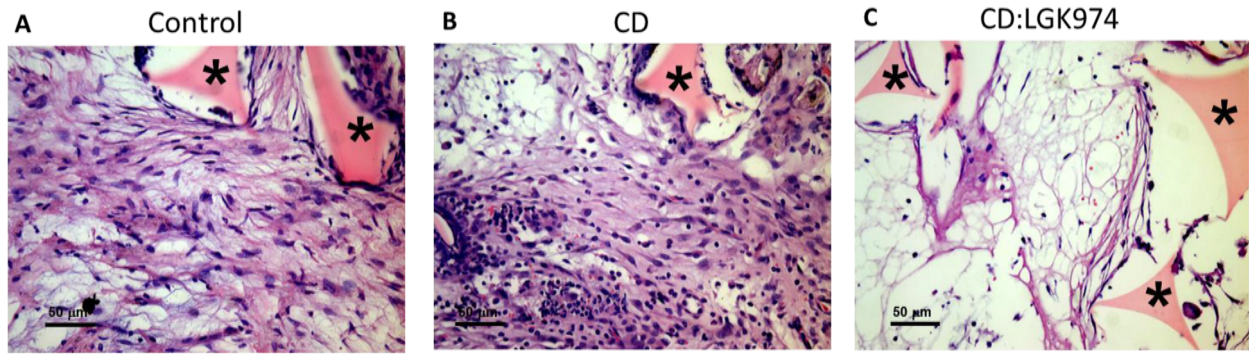
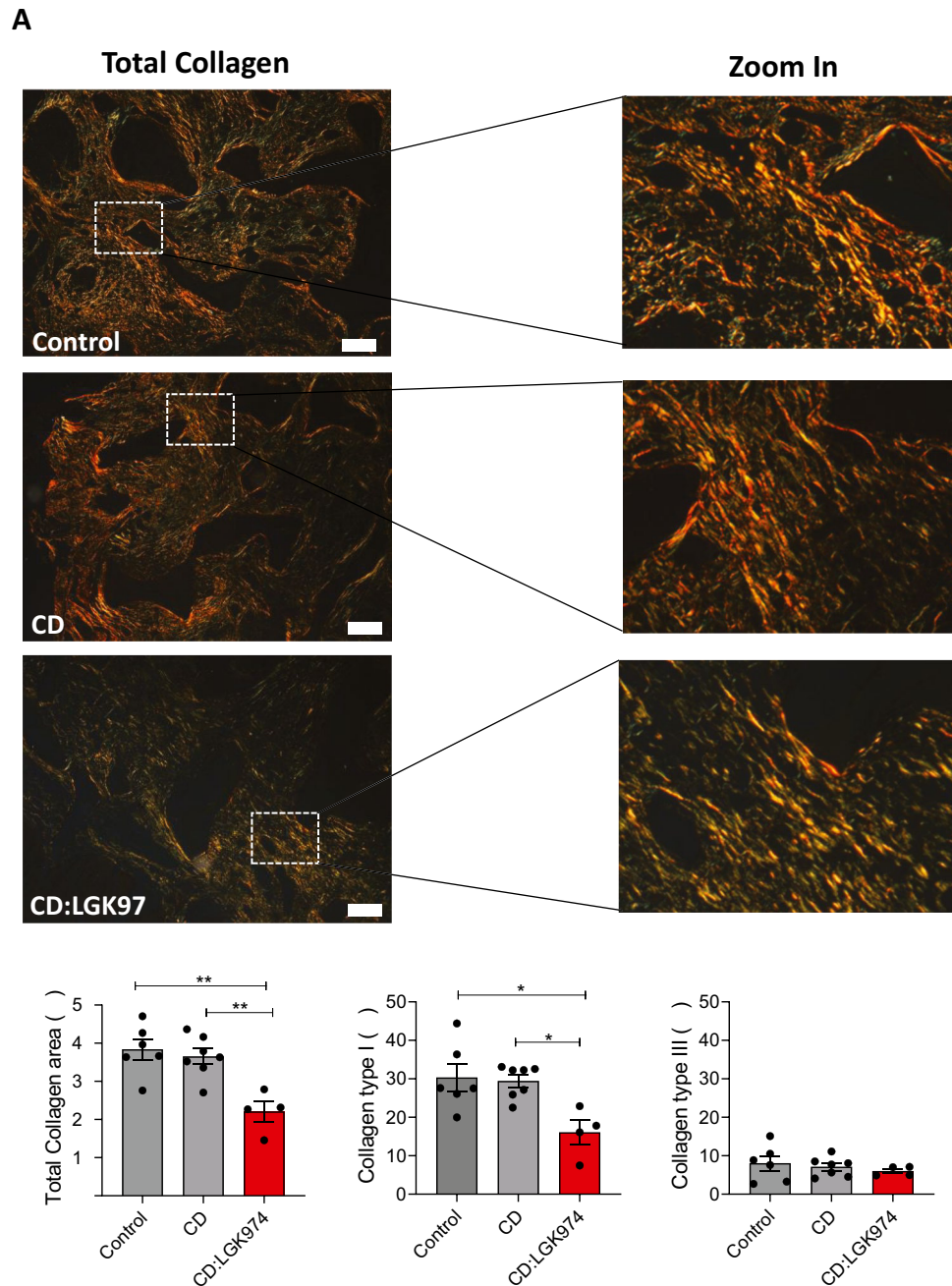


Fig. 6 CD:LGK974 treatment decreased collagen deposition at the implants. Representative histological sections of picrosirius-red stained implants for collagen deposition quantification (total, type I, and type III) using polarized light after 14 days of oral treatment. Inserts show zoomed images of type I collagen fibers (red/orange) and type III collagen fibers (green) in each group. Scale bar, 1 mm. **B** Morphometric analysis of collagen deposition showed a significant decrease in total and type I collagen deposition in mice treated with CD:LGK974 compared to Control and CD groups. Data are mean \pm S.E.M.; One-way ANOVA; * $P < 0.05$



as a carrier. CD increases solubility, facilitates transport across biological barriers, improves bioavailability, and reduces the toxicity of extremely insoluble drugs [25, 26, 43]. Previously, our group characterized the CD:LGK974 complex formation and demonstrated that this complex improves the solubility and bioavailability of LGK974 when administered orally. Because of the improved bioavailability of LGK974 when complexed with β SBECD, a dose of 5 mg/kg/day was used in the present work instead of the usual dose of 10 mg/kg/day, which also reduces the possibility of toxicity caused by LGK974 [25, 41].

The efficacy of treatment with the CD:LGK974 complex was evaluated by observing the development of the foreign body reaction and its components between the Control, CD, and CD:LGK974 groups. Upon arrival at the site, neutrophils adhere to the temporary extracellular matrix around the implant, releasing pro-inflammatory factors such as cytokines (TNF- α , IFN- γ), reactive oxygen species (ROS), and proteolytic enzymes [19]. These cytokines promote the recruitment of dendritic cells and monocytes, triggering differentiation into pro-inflammatory macrophages (M1). Following, the resident macrophages initiate the release of

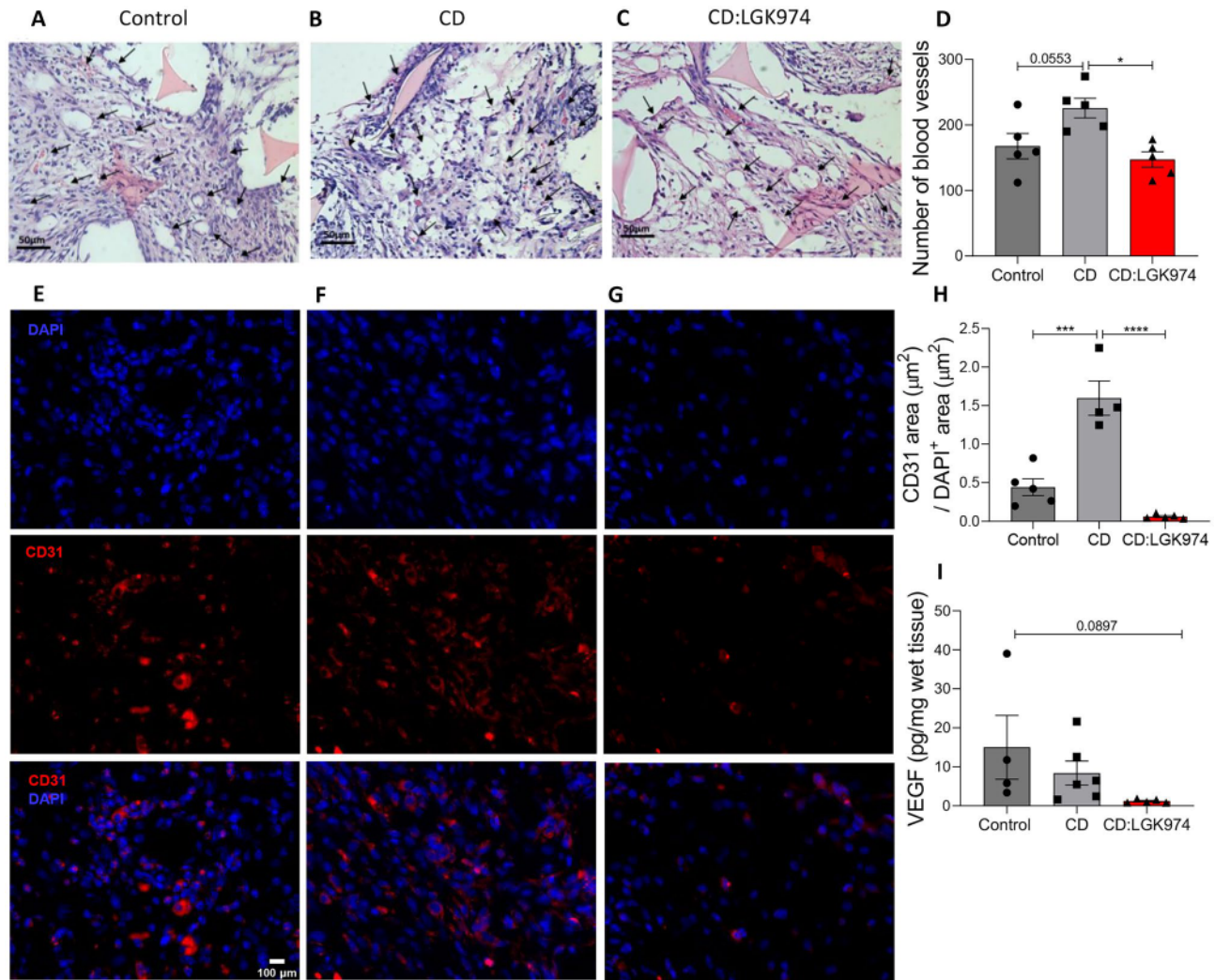


Fig. 7 CD:LGK974 treatment decreased the number of vessels and levels of pro-angiogenic factors. **A–C** Representative H&E sections of implants 14 days after oral treatment (arrows indicate blood vessels). Scale bar, 50 μm . **D** Mice treated with CD:LGK974 showed decreased number of vessels formed at the implant compared to Control and CD groups. **E–G** Representative immunofluorescence of implants 14 days after oral treatment (arrows indicate blood vessels).

E Control: saline; **F** CD; **G** CD:LGK974 (dose: 5 mg/kg/day). Scale bar, 100 μm . **H** Fluorescence quantification of CD31 showed that mice treated with CD:LGK974 showed reduced area of vessels at the implant compared to Control and CD groups. **I** CD:LGK974-treated group exhibited decreased levels of VEGF at the implant compared to Control and CD groups. Data are mean \pm S.E.M.; One-way ANOVA; * $P < 0.05$; *** $P < 0.001$; **** $P < 0.0001$

additional inflammatory factors such as TNF- α and interleukins (IL-1, IL-6, and IL-8) to recruit even more macrophages [19, 44]. Pro-fibrotic macrophages (M2) promote the release of TGF- β 1, which recruits fibroblasts that will adhere to the site and promote extracellular matrix deposition, thus promoting fibrosis and encapsulation of the foreign body [19, 45]. In this way, CD:LGK974 decreased the release of pro-inflammatory cytokines, which reduced the infiltration of immune cells. Furthermore, CD:LGK974 decreased the infiltration of pro-inflammatory and pro-fibrotic (CD206+) neutrophils, monocytes, macrophages, and also dendritic cells (CD11c+), and activated dendritic cells (CD11c+IA-IE+), compared to the other groups. Pro-fibrotic cells were labeled

with the mannose receptor CD206, usually overexpressed in cell of this type [46]. Therefore, our findings using flow cytometry indicate the ability of the complex to reduce the inflammatory process caused by the implantation of the implant at the intraperitoneal site.

The chronification of inflammation—due to a failure to repair the tissue and an increased recruitment of macrophages—results in the fusion of macrophages and the formation of giant cells. The presence of giant cells is one of the characteristics of the foreign body reaction. Giant cells are multinucleated cells with the ability to phagocytize much larger particles (> 10 μm) than a normal phagocyte [19]. Thus, to evaluate the progress of foreign body reaction, we

assessed the number of giant cells in H&E-stained sections and immunofluorescence. Mice treated with CD:LGK974 showed a significantly reduced number of giant cells, formed by macrophages (CD68+) fusion, compared to the Control and CD groups. This corroborated the data about decreased infiltration of inflammatory cells via flow cytometry, especially macrophages.

Furthermore, the chronification of inflammation triggered by the implant also leads to the phenotype change of pro-inflammatory macrophages (M1) to profibrotic macrophages (M2), which stimulates collagen deposition and fibrosis [19]. The progression of fibrosis is related to the upregulation of Wnt signaling, such as the accumulation of β -catenin and consequently increased expression of pro-fibrotic genes and factors such as TGF- β 1 [19, 21]. Thus, to correlate the upregulation of Wnt signaling with increased fibrosis in implants, we dosed some factors directly involved in fibrosis formation via western blot, such as TGF- β 1, β -catenin, and α -SMA protein. Treatment with CD:LGK974 complex significantly decreased β -catenin compared to Control and CD groups, which indicates the inhibition of the Wnt pathway. In addition, treatment with CD:LGK974 complex decreased TGF- β 1 and α -SMA compared to Control and CD groups. Decreased TGF- β 1 levels indicate a lower recruitment and activation of fibroblasts to the implants, which in turn reduces the deposition of extracellular matrix and, consequently, fibrosis [20]. Although the reduction of α -SMA and TGF- β 1 was not statistically significant, the decreasing trend suggests that the inhibition of the Wnt pathway was effective and the reduction of these factors could be enhanced by increasing the complex dose.

We also demonstrated that mice treated with CD:LGK974 had decreased collagen deposition and fibrosis formation at the implant, measured via histological evaluation and fibrotic score. Through these analyses, decreased collagen fiber deposition was found at the implant of mice treated with CD:LGK974 complex. We also demonstrated, quantitatively, that CD:LGK974 reduced total collagen and type I collagen deposition at the implant compared to other groups. The reduced deposition of type III and I collagen at the implants suggests a decreased chronic inflammatory process as well as fibroblast recruitment and activation [19, 47, 48]. Together, our results provide important evidence that CD:LGK974 complex reduces fibrosis in implants at the intraperitoneal site, highlighting its potential as a promising strategy for the treatment of peritoneal fibrosis.

Beyond inflammation, the formation of fibrovascular tissue triggered by the implant also induces the release of pro-angiogenic factors, such as VEGF [9, 10]. These newly formed vessels have the function of nourishing the surrounding tissue and allowing the infiltration of inflammatory cells, which contribute to the encapsulation process

and the complete isolation of the biomaterial [9, 10, 19, 38]. Angiogenic parameters were assessed due to their importance in the resolution of inflammation and fibrosis. Treatment with CD:LGK974 reduced not only VEGF levels but also the number and area of vessels compared to Control and CD groups. Together, these findings suggest that our treatment resulted in a decrease in anoxic stimuli, leading to a reduction in the release of pro-angiogenic factors and as well as the formation of new vessels around the implant.

Here, we confirmed our initial hypothesis that the inhibition of Wnt signaling via CD:LGK974 complex would decrease foreign body reaction and formation of fibrotic tissue over the implant.

Conclusion

In this work, we successfully used a polyether-polyurethane matrix as a model implant to assess the inflammatory, fibrogenic, and angiogenic responses at the intraperitoneal site. These responses were examined in typical (Control) situations, as well as after treatment with CD:LGK974 complex, which acts to limit the progression of the foreign body reaction by inhibiting the Wnt pathway. We demonstrated that oral treatment with CD:LGK974 complex every day for 14 days significantly reduced the inflammatory process that triggers the foreign body reaction at the implanted biomaterial, with the treatment group showing reduced inflammation scores and reduced cytokine levels at the implant site. In addition, treatment with CD:LGK974 complex decreased fibrosis and angiogenesis at the implant, shown by a reduced amount of collagen deposition, a reduced number and area of blood vessels, and reduced levels of VEGF at the implant site. Thus, this work introduces a potentially new application of the Wnt inhibitor complex to limit the negative response to biomaterial implants, reducing peritoneal fibrosis and ultimately reducing rejection of implants at the intraperitoneal site. With this daily oral treatment, biomaterials already used clinically could have improved compatibilities, allowing life-saving therapies to continue past their current lifetimes.

Supplementary Information The online version contains supplementary material available at <https://doi.org/10.1007/s13346-023-01303-0>.

Acknowledgements We would like to thank Laboratório de Ressonância Magnética de Alta Resolução (UFMG/LIPq/LAREMAR/ICEx/DQ) and their staff for the access to their analytical facilities.

Author contribution Pedro Pires Goulart Guimaraes, Ana Luíza de Castro Santos, Silvia Passos Andrade, and Paula Peixoto Campos contributed to the study conception and design. Ana Luíza de Castro Santos, Natália Jordana Alves da Silva, Celso Tarso Rodrigues Viana, Letícia Cristine Cardoso dos Santos, Gabriel Henrique Costa da Silva, Sérgio Ricardo Aluotto Scalzo Júnior, Pedro Augusto Carvalho Costa, Walison da Silva Nunes, Itamar Couto Guedes de Jesus, and Mariana T. Q. de Magalhães, performed experiments and collected data.

Pedro Pires Goulart Guimaraes, Frédéric Frézard, Silvia Guatimosim, Rebecca M. Haley, Michael J. Mitchell, Silvia Passos Andrade, Paula Peixoto Campos, and Mariana T. Q. de Magalhães discussed the results and strategy. The first draft of the manuscript was written by Pedro Pires Goulart Guimaraes, Ana Luíza de Castro Santos, Sérgio Ricardo Aluotto Scalzo Júnior, and Pedro Augusto Carvalho Costa, which was edited by Frédéric Frézard, Silvia Guatimosim, Rebecca M. Haley, Michael J. Mitchell, Silvia Passos Andrade, Paula Peixoto Campos, and Alexander Birbrair. All authors read and approved the final manuscript.

Funding P.P.G.G. is supported by CNPq (401390/2020–9; 442731/2020–5), CAPES (88887.513270/2020–00), and FAPEMIG (Rede de Pesquisa Imunobiofar RED-00202-22, Universal 2021 APQ-00826–21). M.J.M. receives support from a Burroughs Wellcome Fund Career Award at the Scientific Interface (CASI) and a U.S. National Institutes of Health (NIH) Director’s New Innovator Award (DP2 TR002776). R.M.H. receives support from the National Science Foundation Graduate Research Fellowship (NSF-GRFP).

Availability of data and materials The datasets generated during and/or analyzed during the current study are available from the corresponding author on reasonable request.

Declarations

Ethics approval and consent to participate The protocols for animal experimentation were approved by the Ethics Committee at the Federal University of Minas Gerais (CEUA/UFGM) (Protocol No. 282/2018). All procedures were performed following the standards established in the guidelines and policies of the National Institutes of Health (NIH) Guide for the Care and Use of Laboratory Animals.

Consent for publication Not applicable. No human studies have been performed in this research.

Competing interests The authors declare no competing interests.

References

- Ratner BD, Zhang G. A history of biomaterials, Fourth Ed. Elsevier. 2020. <https://doi.org/10.1016/b978-0-12-816137-1.00002-7>.
- Zhou G, Groth T. Host responses to biomaterials and anti-inflammatory design—a brief review. *Macromol Biosci*. 2018;18(8):1800112. <https://doi.org/10.1002/mabi.201800112>.
- Kohane DS, Langer R. Polymeric biomaterials in tissue engineering. *Pediatr Res*. 2008;63:487–91. <https://doi.org/10.1203/01.pdr.0000305937.26105.e7>.
- Yu X, Tang X, Gohil SV, Laurencin CT. Biomaterials for bone regenerative engineering. *Adv Healthc Mater*. 2015;4:1268–85. <https://doi.org/10.1002/adhm.201400760>.
- Bose S, Volpatti LR, Thiono D, Yesilyurt V, McGladrigan C, Tang Y, Facklam A, Wang A, Jhunjhunwala S, Veiseh O, Hollister-Lock J, Bhattacharya C, Weir GC, Greiner DL, Langer R, Anderson DG. A retrievable implant for the long-term encapsulation and survival of therapeutic xenogeneic cells. *Nat Biomed Eng*. 2020;4:814–26. <https://doi.org/10.1038/s41551-020-0538-5>.
- He J, Renard E, Lord P, Cohen D, Gu B, Wang X, Yenduri G, Burgess DJ. Strategies for extended lifetime of implantable intraperitoneal insulin catheters. *J Control Release*. 2022;341:487–97. <https://doi.org/10.1016/j.jconrel.2021.11.038>.
- Veiseh O, Doloff JC, Ma M, Vegas AJ, Tam HH, Bader AR, Li J, Langan E, Wyckoff J, Loo WS, Jhunjhunwala S, Chiu A, Siebert S, Tang K, Hollister-Lock J, Aresta-Dasilva S, Bochenek M, Mendoza-Elias J, Wang Y, Qi M, Lavin DM, Chen M, Dholakia N, Thakrar R, Lacík I, Weir GC, Oberholzer J, Greiner DL, Langer R, Anderson DG. Size- and shape-dependent foreign body immune response to materials implanted in rodents and non-human primates. *Nat Mater*. 2015;14:643–51. <https://doi.org/10.1038/nmat4290>.
- Franz S, Rammelt S, Scharnweber D, Simon JC. Immune responses to implants—a review of the implications for the design of immunomodulatory biomaterials. *Biomaterials*. 2011;32:6692–709. <https://doi.org/10.1016/j.biomaterials.2011.05.078>.
- Campos PP, Andrade SP, Moro L, Ferreira MA, Vasconcelos AC. Cellular proliferation, differentiation and apoptosis in polyether-polyurethane sponge implant model in mice. *Histol Histopathol*. 2006;21:1263–1270. <https://doi.org/10.14670/HH-21.1263>.
- Castro PR, Marques SM, Campos PP, Cardoso CC, Sampaio FP, Ferreira MAND, Andrade SP. Kinetics of implant-induced inflammatory angiogenesis in abdominal muscle wall in mice. *Microvasc Res*. 2012;84:9–15. <https://doi.org/10.1016/j.mvr.2012.04.003>.
- Pereira LX, Viana CT, Orellano LA, Almeida SA, Vasconcelos AC, de Miranda Goes A, Birbrair A, Andrade SP, Campos PP. Synthetic matrix of polyether-polyurethane as a biological platform for pancreatic regeneration. *Life Sci*. 2017;176:67–74. <https://doi.org/10.1016/j.lfs.2017.03.015>.
- Duxbury PJ, Harvey JR. Systematic review of the effectiveness of polyurethane-coated compared with textured silicone implants in breast surgery. *J Plast Reconstr Aesthetic Surg*. 2016;69:452–60. <https://doi.org/10.1016/j.bjps.2016.01.013>.
- Alzahrani K, Lejeune J, Lakhil W, Morel B, Cook AR, Braïk K, Lardy H, Binet A. Polyurethane versus silicone port a cath: what’s going on at removal? *J Pediatr Surg*. 2018;53:1417–9. <https://doi.org/10.1016/j.jpedsurg.2017.06.025>.
- Laurano R, Boffito M, Abrami M, Grassi M, Zoso A, Chiono V, Ciardelli G. Dual stimuli-responsive polyurethane-based hydrogels as smart drug delivery carriers for the advanced treatment of chronic skin wounds. *Bioact Mater*. 2021;6:3013–24. <https://doi.org/10.1016/j.bioactmat.2021.01.003>.
- Pontes GH, Carneiro Filho FS, Vargas Guerrero LA, Lipinski LC, de Noronha L, Silva EN, Serra-Guimarães F. Reduced remodeling biomarkers tissue expression in nanotextured compared with polyurethane implants capsules: a study in rats. *Aesthetic Surg J*. 2021;41:NP664–NP683. <https://doi.org/10.1093/asj/sjaa315>.
- Mendes JB, Campos PP, Ferreira MA, Bakhle YS, Andrade SP. Host response to sponge implants differs between subcutaneous and intraperitoneal sites in mice. *J Biomed Mater Res. Part B Appl Biomater*. 2007;83:408–415. <https://doi.org/10.1002/jbm.b.30810>.
- Terri M, Trionfetti F, Montaldo C, Cordani M, Tripodi M, Lopez-Cabrera M, Strippoli R. Mechanisms of peritoneal fibrosis: focus on immune cells–peritoneal stroma interactions. *Front Immunol*. 2021;12:1–17. <https://doi.org/10.3389/fimmu.2021.607204>.
- Abul AHL, ABBAS K. Patologia básica - Robbins e Cotran. 2016.
- Carnicer-Lombarte A, Chen ST, Malliaras GG, Barone DG. Foreign body reaction to implanted biomaterials and its impact in nerve neuroprosthetics. *Front Bioeng Biotechnol*. 2021;9:1–22. <https://doi.org/10.3389/fbioe.2021.622524>.
- Noskovicova N, Hinz B, Pakshir P. Implant fibrosis and the underappreciated role of myofibroblasts in the foreign body reaction. *Cells*. 2021;10. <https://doi.org/10.3390/cells10071794>.
- Burgy O, Königshoff M. The WNT signaling pathways in wound healing and fibrosis. *Matrix Biol*. 2018;68–69:67–80. <https://doi.org/10.1016/j.matbio.2018.03.017>.
- Jung Y, Park J. Wnt signaling in cancer : therapeutic targeting of Wnt signaling beyond β -catenin and the destruction complex. *Exp Mol Med*. 2020;52:183–91. <https://doi.org/10.1038/s12276-020-03806>.

23. Guo Y, Sun L, Xiao L, Gou R, Fang Y, Liang Y, Wang R, Li N, Liu F, Tang L. Aberrant Wnt/beta-catenin pathway activation in dialysate-induced peritoneal fibrosis. *Front Pharmacol.* 2017;8:774. <https://doi.org/10.3389/fphar.2017.00774>.
24. Nusse R, Clevers H. Wnt/ β -catenin signaling, disease, and emerging therapeutic modalities. *Cell.* 2017;169(6):985–999. <https://doi.org/10.1016/j.cell.2017.05.016>.
25. Guimaraes PPG, Tan M, Tammela T, Wu K, Chung A, Oberli M, Wang K, Spektor R, Riley RS, Viana CTR, Jacks T, Langer R, Mitchell MJ. Potent in vivo lung cancer Wnt signaling inhibition via cyclodextrin-LGK974 inclusion complexes. *J Control Release.* 2018;290:75–87. <https://doi.org/10.1016/j.jconrel.2018.09.025>.
26. Stella VJ, Rajewski RA. Cyclodextrins: their future in drug formulation and delivery. *Pharm Res.* 1997;14:556–67. <https://doi.org/10.1023/A:1012136608249>.
27. Szejtli J. Medicinal applications of cyclodextrins. *Med Res Rev.* 1994;14:353–86. <https://doi.org/10.1002/med.2610140304>.
28. Hirayama F, Uekama K. Cyclodextrin-based controlled drug release system. *Adv Drug Deliv Rev.* 1999;36(1):125–141. [https://doi.org/10.1016/S0169-409X\(98\)00058-1](https://doi.org/10.1016/S0169-409X(98)00058-1).
29. Andrade SP, Machado RDP, Teixeira AS, Belo AV, Tarso AM, Beraldo WT. Sponge-induced angiogenesis in mice and the pharmacological reactivity of the neovasculature quantitated by a fluorimetric method. *Microvasc Res.* 1997;54:253–61. <https://doi.org/10.1006/mvre.1997.2047>.
30. Thompson K, Maltby J, Fallowfield J, Mcaulay M, Millward-Sadler H, Sheron N. Interleukin-10 expression and function in experimental murine liver inflammation and fibrosis. *Hepatology.* 1998;28:1597–606. <https://doi.org/10.1002/hep.510280620>.
31. Li JP, Gao Y, Chu SF, Zhang Z, Xia CY, Mou Z, Song XY, He WB, Guo XF, Chen NH. Nrf2 pathway activation contributes to anti-fibrosis effects of ginsenoside Rg1 in a rat model of alcoholand CCl4-induced hepatic fibrosis. *Acta Pharmacol Sin.* 2014;35:1031–1044. <https://doi.org/10.1038/aps.2014.41>.
32. Junqueira LC, Bignolas G, Brentani RR. Picrosirius staining plus polarization microscopy, a specific method for collagen detection in tissue sections. *Histochem J.* 1979;11:447–455. <http://www.ncbi.nlm.nih.gov/pubmed/7344781>.
33. Otsu N. A Threshold selection method from gray-level histograms. *IEEE Trans Syst Man Cybern.* 1979;9:62–6. <https://doi.org/10.1109/TSMC.1979.4310076>.
34. Canny J. A computational approach to edge detection. *IEEE Trans Pattern Anal Mach Intell PAMI-8.* 1986:679–698. <https://doi.org/10.1109/TPAMI.1986.4767851>.
35. Schneider HJ, Hacket F, Rüdiger V, Ikeda H. NMR studies of cyclodextrins and cyclodextrin complexes. *Chem Rev.* 1998;98:1755–85. <https://doi.org/10.1021/cr970019t>.
36. Anderson JM, Rodriguez A, Chang DT. Foreign body reaction to biomaterials. *Semin Immunol.* 2008;20:86–100. <https://doi.org/10.1016/j.smim.2007.11.004>.
37. Chu C, Liu L, Rung S, Wang Y, Ma Y, Hu C, Zhao X, Man Y, Qu Y. Modulation of foreign body reaction and macrophage phenotypes concerning microenvironment. *J Biomed Mater Res Part A.* 2020;108:127–35. <https://doi.org/10.1002/jbma.36798>.
38. Mariani E, Lisignoli G, Borzi RM, Pulsatelli L. Biomaterials: foreign bodies or tuners for the immune response? *Int J Mol Sci.* 2019;20. <https://doi.org/10.3390/ijms20030636>.
39. Kobayashi A, Suzuki Y, Sugai S. Specificity of transaminase activities in the prediction of drug-induced hepatotoxicity. *J Toxicol Sci.* 2020;45:515–37. <https://doi.org/10.2131/jts.45.515>.
40. Ratner AS, Hoffman BD. Biomaterials science - an introduction to materials in medicine. 1996.
41. Liu J, Pan S, Hsieh MH, Ng N, Sun F, Wang T, Kasibhatla S, Vanasse G, Harris JL. Targeting Wnt-driven cancer through the inhibition of Porcupine by LGK974. 2013;110:20224–20229. <https://doi.org/10.1073/pnas.1314239110>.
42. Feng Y, Ren J, Gui Y, Wei W, Shu B, Lu Q, Xue X, Sun X. Wnt / b -Catenin – promoted macrophage alternative activation contributes to kidney fibrosis. 2018;182–193. <https://doi.org/10.1681/ASN.2017040391>.
43. Webber MJ, Langer R. Drug delivery by supramolecular design. *Chem Soc Rev.* 2017;46:6600–20. <https://doi.org/10.1039/c7cs00391a>.
44. Geissmann F, Manz MG, Jung S, Sieweke MH, Merad M, Ley K. Development of monocytes, macrophages, and dendritic cells. *Science.* 2010;327(80):656–661. <https://doi.org/10.1126/science.1178331>.
45. Yunna C, Mengru H, Lei W, Weidong C. Macrophage M1/M2 polarization. *Eur J Pharmacol.* 2020;877:173090. <https://doi.org/10.1016/j.ejphar.2020.173090>.
46. Shapouri-Moghaddam A, Mohammadian S, Vazini H, Taghadosi M, Esmaili SA, Mardani F, Seifi B, Mohammadi A, Afshari JT, Sahebkar A. Macrophage plasticity, polarization, and function in health and disease. 2018. <https://doi.org/10.1002/jcp.26429>.
47. Diegelmann RF. Cellular biochemical aspects of normal and abnormal wound healing: an overview. *J Urol.* 1997;157:298–302. [https://doi.org/10.1016/S0022-5347\(01\)65364-3](https://doi.org/10.1016/S0022-5347(01)65364-3).
48. Piersma B, Bank RA, Boersema M. Signaling in fibrosis: TGF- β , WNT, and YAP/TAZ converge. *Front Med.* 2015;2:59. <https://doi.org/10.3389/fmed.2015.00059>.

Publisher's Note Springer Nature remains neutral with regard to jurisdictional claims in published maps and institutional affiliations.

Springer Nature or its licensor (e.g. a society or other partner) holds exclusive rights to this article under a publishing agreement with the author(s) or other rightsholder(s); author self-archiving of the accepted manuscript version of this article is solely governed by the terms of such publishing agreement and applicable law.